

Machine Learning Approaches for Super-resolution Problems

SENSE Research Experience Placement Report

Qi Qiu

Supervisor: Dr. Stuart King

August 2023

Abstract

Synthetic Aperture Radar (SAR) is widely used in remote sensing, providing all-weather imaging unaffected by cloud cover, rain, and smoke. Employed in various satellite platforms, SAR offers valuable terrain observations at distinct levels of resolution. This research is focused on utilizing data from two different SAR sources: the Sentinel-1 satellite, which captures wide-ranging but low-resolution SAR imagery, and Capella Space, offering high-resolution SAR images with limited coverage. The study is specifically centered around the Turkey earthquake region, with Gaziantep city as the focal area of interest. By integrating machine learning techniques using python, the study aims to investigate the feasibility of generating high-resolution satellite images from lower-resolution inputs. The primary objective is to enhance the spatial resolution of SAR imagery, thereby unlocking its potential for advanced disaster response and precise environmental monitoring.

Keywords: Remote Sensing, Satellite Imagery, Disaster Response

Contents

1	Background	3
2	Introduction	4
2.1	Synthetic Aperture Radar	4
2.1.1	Electromagnetic Spectrum	4
2.1.2	Polarizations	5
2.1.3	Backscatter	6
2.2	Data sources: Capella Space and Sentinel-1	6
2.3	Georeferenced Raster Imagery	8
2.4	Image Resizing Techniques	9
2.4.1	Bilinear Interpolation	9
2.4.2	Bicubic Interpolation	10
3	Sentinel-1 Preprocessing	11
3.1	Thermal/Border Noise Removal	11
3.2	Radiometric Calibration	12
3.3	Speckle Filtering	12
4	Approach 1: pairing Sentinel-1 data with Capella data	13
4.1	Image Resizing	13
4.2	Pixel Alignment	13
5	Approach 2: Simulate a Sentinel-1 Image Data	15
5.1	Simulation Based on Capella Image	15
5.2	Gaussian Blur and Image Entropy	16
6	Machine Learning Models	17
6.1	Model Selections	17
6.1.1	Random Forest	17
6.1.2	Gradient Boosting Random Forest	18
6.1.3	Decision Tree	19
6.2	Feature Vectors Preparation	19
6.2.1	Surrounding Pixel Values	19
6.2.2	RGBI Band Pixel Values from Sentinel-2	20
6.2.3	Calculation of GNDVI, NDVI, and Building Index	20
6.2.4	Integration of Building Layer from OpenStreetMap	21
6.3	Principal Component Analysis	22
6.4	Evaluation Metrics for Model Performance	23
7	Results and Analysis	24
7.1	Approach 1: pairing Sentinel-1 data with Capella data	24
7.1.1	Enhancing Super Resolution: EDSRx2 Upscaling	24
7.2	Approach 2: Simulate a Sentinel-1 Image Data	25
8	Conclusion	26
References		27

1 Background

Synthetic Aperture Radar (SAR) technology has emerged as a powerful tool in the realm of remote sensing and mapping of Earth surfaces. Unlike traditional optical sensors, SAR utilizes radio waves to capture relatively high-resolution images even in challenging weather conditions (Ager 2013). This distinctive capability has made SAR an indispensable asset in various applications, including environment monitoring such as oil spills (Bing et al. 2019), flooding (Smith 2002), urban growth (Sanderson 2001).

However, the resolution of SAR images often remains constrained by the limitations of imaging equipment and various uncontrollable factors, rendering them insufficient for practical applications (C. Zhang et al. 2023). As a result, enhancing the resolution of SAR images has emerged as a prominent and vital research focus within the field of SAR image processing(Li et al. 2021).

Given the diverse range of satellites and remote sensor technologies, it is common to encounter inconsistent spatial resolutions between source datasets and target results for specific tasks (L. Zhang et al. 2021). Hence, achieving super-resolution results from relatively low-resolution remotely sensed images holds immense value.

To address the challenge of resolution inconsistency in images, a commonly employed approach is interpolation during the preprocessing stage. This involves methods such as bilinear and bicubic interpolation (Amara, Bandara, and Silva 2018). However, interpolation-based techniques have drawbacks, particularly in areas with edges and high-frequency details, where the spatial information loss and insufficient gradients become evident (L. Zhang et al. 2021). In this study, we opt to utilize bilinear interpolation to preprocess and prepare the satellite images for model training.

By harnessing supervised machine learning algorithms, this research seeks to explore the potential of generating high-resolution SAR images from lower-resolution inputs. The utilization of machine learning models, such as random forests, gradient boosting, and decision tree with principal component analysis, promises to explore new possibilities for SAR image enhancement and subsequent applications. The study explores two distinct approaches to prepare the inputs and outputs for the ML models to achieve this goal: pairing lower-resolution Sentinel-1 SAR data with higher-resolution Capella Space SAR data and simulating Sentinel-1 data using advanced image processing techniques.

With the specific focus on the Turkey earthquake region, particularly Gaziantep city, this research aims to contribute to disaster response and environmental monitoring in the context of the Sentinel-1¹ and Capella Space SAR datasets². By advancing super resolution techniques in SAR imaging, this study aspires to expand the utility and impact of SAR technology in critical Earth observation endeavors.

The subsequent sections of this research report will delve into the methodology, data preprocessing, and machine learning models employed to achieve the objectives. The results and analysis section will showcase the outcomes of each approach, followed by a comprehensive discussion, conclusion, and potential directions for future research. Through these efforts, this research endeavors to

¹Copernicus Sentinel data 2023. Retrieved from Copernicus Open Access Hub on July 6, 2024, processed by ESA.

²Capella Space Synthetic Aperture Radar (SAR) Open Dataset was accessed on July 6, 2024 from https://registry.opendata.aws/capella_opendata.

propel SAR imaging to new heights and foster advancements in the field of remote sensing and geospatial analysis.

2 Introduction

In the realm of remote sensing, passive optical images from well-known sources like Landsat, Moderate Resolution Imaging Spectroradiometer (MODIS), and Sentinel-2 have long been familiar to scientists. However, a growing area of interest lies in Synthetic Aperture Radar (SAR), a type of active remote sensing data that is gaining prominence.

2.1 Synthetic Aperture Radar

SAR operates differently from optical imagery, which can be demonstrated by Figure 1, as it involves the sensor emitting its own energy and then capturing the reflected energy after interacting with the Earth's surface.

The spatial resolution of radar data is determined by the ratio of the sensor's wavelength to the length of its antenna ([özdemir 2012](#)). A longer antenna results in higher spatial resolution. However, achieving very high resolution with a long antenna is impractical for satellites in space. To overcome this limitation, the concept of synthetic aperture has been employed. By combining a sequence of acquisitions from a shorter antenna, they simulate a larger antenna, enabling the capture of higher resolution data, which provides valuable insights without the need for an excessively large physical antenna ([Berens 2006](#)).

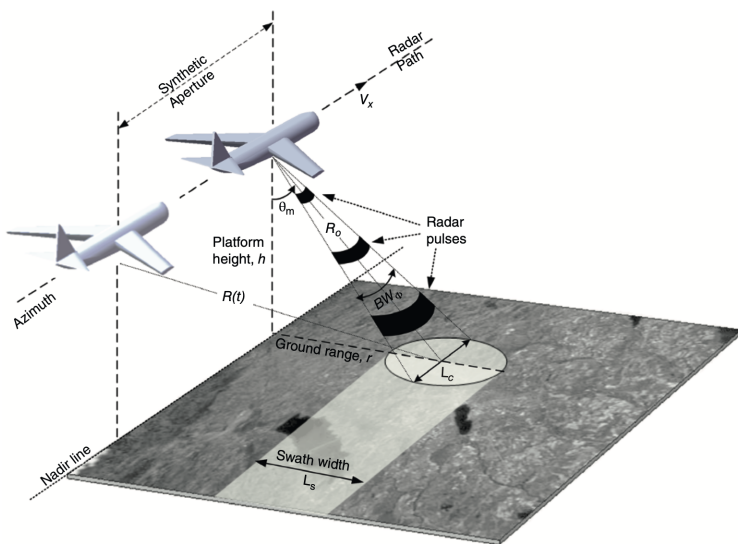


Figure 1: Geometry of observations used by a SAR satellite. Taken from [özdemir \(2012\)](#).

2.1.1 Electromagnetic Spectrum

SAR operates in the microwave band of the electromagnetic spectrum, which is demonstrated by Figure 2, granting it the capability to penetrate the atmosphere in various weather conditions. Unlike optical sensors that utilize wavelengths ranging from visible to thermal infrared waves, SAR sensors work with longer microwaves, spanning from K-band to P-band ([Menezes and Barba-Sevilla 2023](#)). These microwave wavelengths offer valuable insights into the physical properties of

the Earth's surface, including roughness, density, and moisture content.

The distinct scattering behavior of microwave wavelengths is a key factor. Depending on the feature reflecting them, microwave wavelengths scatter differently. If the wavelength exceeds the size of the feature of interest, the electromagnetic wave will not detect it. This characteristic allows SAR to gather specific information about the Earth's surface based on how microwaves interact with different surface properties (NASA n.d.).

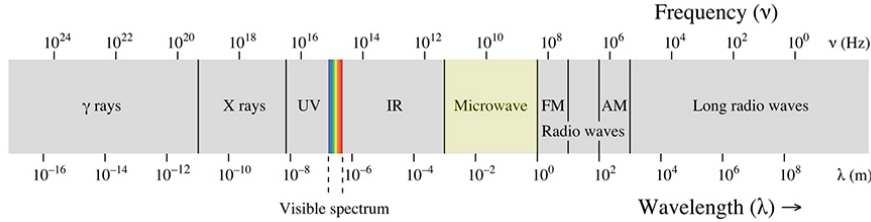


Figure 2: The electromagnetic spectrum. Credit: Alaska Satellite Facility.

2.1.2 Polarizations

SAR sensors exhibit different polarization capabilities, determining the polarization of the transmitted and received electromagnetic waves. Single-pol sensors employ a single polarization (VV or HH) for signal transmission and measurement. In contrast, dual-pol sensors use both co-polarized (VV, HH) and cross-polarized (VH, HV) returns (özdemir 2012). Additionally, quad-pol sensors possess full quad-polar capabilities, transmitting chirps with both horizontal and vertical polarizations (VV, VH, HV, HH).

The polarization of SAR data is denoted by two letters, indicating the transmitted and received polarizations. Co-polarized data involves transmitted and received waves sharing the same polarization (VV or HH), while cross-polarized data has transmitted and received waves with different polarizations (VH or HV). Dual-polarized SAR images capture either VV and VH polarized data or HH and HV polarized data.

It is crucial to consider the transmitted and received polarization used, as it strongly influences the features captured in the SAR image. By controlling polarization, SAR sensors can highlight distinct characteristics on the Earth's surface based on backscatter behavior.

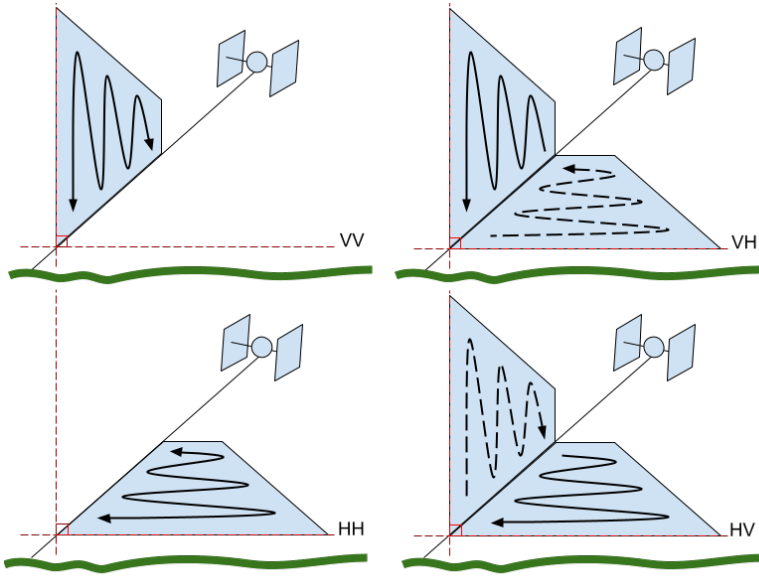


Figure 3: Four different polarization combinations. Credit: Alaska Satellite Facility.

2.1.3 Backscatter

The measured backscatter is the electromagnetic wave received by the SAR sensor, where strong backscatter corresponds to a high digital number, and weak backscatter to a low digital number.

Four main types of scattering mechanisms influence SAR images (NASA 2019):

- 1) Single-Bounce Scattering: Radar signal reflects once off a smooth surface, resulting in low backscatter in both co-polarized and cross-polarized bands.
- 2) Double-Bounce Scattering: Radar signal reflects twice, off a vertical target and then a smooth surface, causing high co-polarized and low cross-polarized backscatter.
- 3) Diffuse Scattering: Radar signal reflects off a rough surface, scattering in various directions, with higher backscatter from rougher surfaces.
- 4) Volume Scattering: Radar signal reflects multiple times off 3D features, randomly changing polarization during reflection. Volume scattering occurs within canopies of short or sparse vegetation.

2.2 Data sources: Capella Space and Sentinel-1

For this research, we have carefully selected Synthetic Aperture Radar (SAR) image data acquired over Gaziantep city on July 4th, 2023, sourced from two prominent providers: Sentinel-1 and Capella Space.

Capella Space offers various SAR products, such as the Single Look Complex (SLC) Product and the Geocoded Terrain Corrected (GEO) Product (Capella 2023). The SLC SAR product includes amplitude and phase data, producing a focused SAR image in slant-range geometry using orbit data for precise georeferencing through Range-Doppler projection. On the other hand, the GEO product exclusively presents amplitude information and undergoes range compression, detection,

focusing, and multi-looking techniques. The multi-look processing improves the radiometric resolution, making it highly suitable for georeferencing applications.

To achieve georeferencing accuracy, the GEO product employs a high-resolution Digital Elevation Model (DEM) for precise terrain-height correction and it is then projected onto the Universal Transverse Mercator (UTM) coordinate system. The GEO product was thoughtfully chosen for its applicability and relevance to the research study.

The Capella SAR images are characterized by linear polarization, with the electric vector oriented horizontally in antenna coordinates. Among the two vertical transmit options available, we selected horizontal receive polarization (HH) for this research.

The resolution of Capella SAR images is approximately 0.35 meters, with each pixel representing a 0.35-meter square on the ground. This high spatial resolution promises to provide detailed insights into the study area.



Figure 4: City Gaziantep: SAR image from Capella Space. Credit: Capella Space.

Similarly, Sentinel-1 SAR images are delivered in two primary product types: Ground Range Detected (GRD) and Single Look Complex (SLC) (ESA [n.d.](#)). For the purpose of this research, we focus on the GRD product. This product type comprises real-valued arrays, indicating backscatter amplitude.

The Sentinel-1 SAR images exhibit linear polarization, with the electric vector oriented vertically in antenna coordinates. Among the two vertical transmit options available, we opted for vertical receive polarization (VV) due to its better overlap with Capella image data.

The resolution of Sentinel-1 SAR images is approximately 10 meters, with each pixel representing a 10-meter square on the ground. Despite its relatively lower resolution compared to Capella, Sentinel-1 provides extensive coverage, making it an essential dataset for our research.

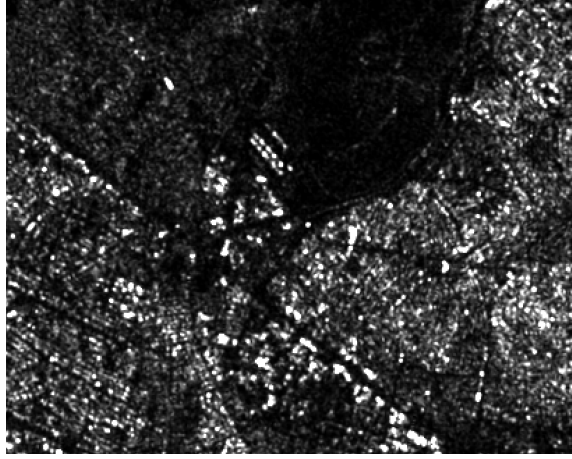


Figure 5: City Gaziantep: SAR image from Sentinel-1. Credit: ESA.

The combination of Sentinel-1 and Capella SAR data offers a unique opportunity to explore super resolution techniques and enhance the spatial resolution of SAR images, enabling comprehensive analysis and interpretation of the study area in Gaziantep city.

2.3 Georeferenced Raster Imagery

The images data from both data sources are georeferenced raster imagery in GeoTIFF format. GeoTIFF is a preferred file format in the geospatial community due to its ability to store both visual pixel data and essential geospatial information within a single file. This unique combination allows for seamless integration of the imagery into Geographic Information Systems (GIS) and facilitates precise analysis and interpretation of the Earth's surface (Freeman, Green, and Hassell 1994).

Below, we provide a detailed explanation of the characteristics of georeferenced raster imagery in GeoTIFF format:

1) Spatial Extent:

Spatial extent refers to the geographical coverage area depicted in the GeoTIFF image. It defines the boundaries of the region captured in the raster image, providing crucial information for accurately aligning the imagery with other spatial datasets and ensuring spatial consistency in geospatial analyses.

2) Coordinate Reference System (CRS):

The Coordinate Reference System (CRS) is a fundamental component of GeoTIFF imagery, defining the spatial reference framework used to represent the geographic location of each pixel in the image. It specifies the coordinate system, units of measurement, and the origin of the coordinate system relative to the Earth's surface. The CRS ensures proper georeferencing and accurate positioning of the image on the Earth's map.

3) Resolution:

Resolution signifies the level of detail captured in each pixel of the GeoTIFF raster image. It quantifies the size of the area represented by a single pixel on the ground. Higher resolution values yield finer details but require larger data storage, while lower resolution values cover larger areas but may sacrifice some finer features.

4) Nodata Value:

The Nodata value represents the absence of valid data within the GeoTIFF image. It is a designated value used to indicate pixels where information is missing or cannot be determined.

Nodata values are critical for data processing and analysis, ensuring that algorithms handle missing data appropriately and do not incorporate them in calculations or visualizations.

5) Multiband Capability:

GeoTIFF format supports the storage of multiple bands (layers) of information within a single file. This capability is particularly useful when dealing with multi-spectral imagery, as it enables the simultaneous representation of different characteristics of the Earth's surface in a single dataset. For instance, SAR imagery from Sentinel-1 and Capella Space often contains dual-polarization data (VV, VH, HH, HV), providing valuable insights into the physical properties of the observed area.

The combination of these characteristics in GeoTIFF format empowers researchers and GIS professionals to conduct in-depth spatial analyses, overlay the imagery with various geographic datasets, and extract meaningful information for a wide range of applications, including land cover classification, change detection, environmental monitoring, and disaster response. Georeferenced raster imagery in GeoTIFF format serves as a cornerstone for geospatial research and supports informed decision-making across diverse domains.

2.4 Image Resizing Techniques

In this research, we have selected bilinear interpolation as the image resizing technique to alter the pixel size during the super resolution process.

2.4.1 Bilinear Interpolation

Bilinear interpolation is a widely used mathematical method that estimates the values of new pixels in an image by considering the values of neighboring pixels. The underlying principle of bilinear interpolation is that pixel intensities change linearly across the image, and it operates on a 2x2 neighborhood of pixels to compute the values of the new pixels (Szeliski 2011).

The methodology of bilinear interpolation, demonstrated by Figure 6, involves the following steps (Weiser and Zarantonello 1988):

1) Determining the Position of New Pixels:

When resizing an image to a higher resolution, the positions of the new pixels in the resized image are determined using bilinear interpolation. Each new pixel is mapped to a corresponding position in the original image based on a transformation matrix.

2) Calculating the Pixel Intensities:

Bilinear interpolation estimates the intensities of the new pixels by taking into account the intensities of the four nearest neighboring pixels in the original image. These neighboring pixels form a 2x2 grid surrounding the new pixel.

3) Computing Weighted Averages:

The intensity of each new pixel is computed as a weighted average of the intensities of its neighboring pixels using formula 1. The weights assigned to the neighboring pixels depend on their distance to the new pixel. Closer neighboring pixels have higher weights in the interpolation process.

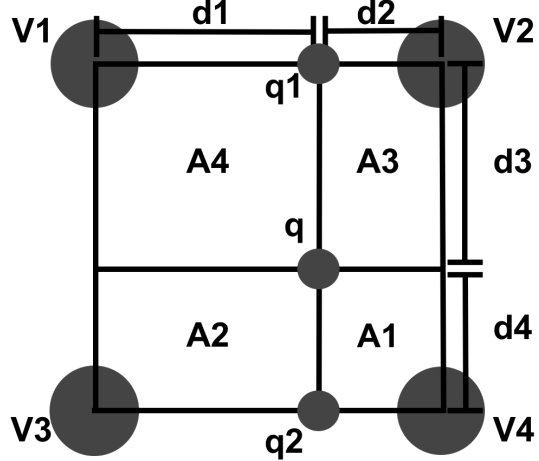


Figure 6: Bilinear interpolation. Credit: Wikipedia.

$$q_1 = V_1 \cdot d_2 + V_2 \cdot d_1, \quad q_2 = V_3 \cdot d_2 + V_4 \cdot d_1, \quad q = q_1 \cdot d_4 + q_2 \cdot d_3 \quad (1)$$

Bilinear interpolation effectively fills in the gaps between original pixels, resulting in a smooth and continuous image. Its straightforward approach makes it suitable for resizing SAR imagery.

2.4.2 Bicubic Interpolation

While bilinear interpolation offers a lightweight and computationally efficient approach for image resizing, it is essential to consider alternative methods, such as bicubic interpolation, to assess their respective performance and suitability for the super resolution task.

Bicubic interpolation is a more complex interpolation technique that considers a larger neighborhood of 4x4 pixels instead of the 2x2 neighborhood used in bilinear interpolation. This larger neighborhood allows bicubic interpolation to capture more intricate patterns and smoothness in the image, potentially resulting in higher quality upscaled images (Sekar, Duraisamy, and Remimol 2014).

Mathematically, the formula for bicubic interpolation is as follows:

$$P(x, y) = \sum_{i=-1}^2 \sum_{j=-1}^2 w(i) \cdot w(j) \cdot I(x + i, y + j) \quad (2)$$

Here, $P(x, y)$ represents the pixel value at the upsampled location, $I(x + i, y + j)$ stands for the pixel value at the neighboring coordinates, and $w(i)$ and $w(j)$ are the weights assigned based on the distance from the original pixel location.

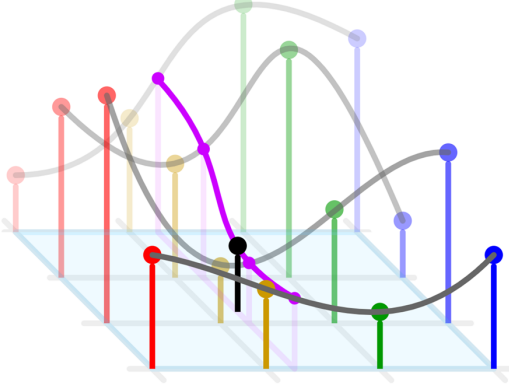


Figure 7: Bicubic interpolation. Credit: Wikipedia.

However, the increased computational complexity of bicubic interpolation can be a significant drawback, especially when dealing with large datasets or real-time applications. In contrast, bilinear interpolation strikes a balance between computational efficiency and image quality, making it a practical choice for our super resolution research.

Furthermore, bilinear interpolation generally exhibits less blurring compared to bicubic interpolation, which is advantageous when working with SAR imagery that requires preserving fine details and features.

In conclusion, bilinear interpolation is chosen as the image resizing technique for its simplicity, efficiency, and ability to provide satisfactory results for enhancing the resolution of SAR images. While bicubic interpolation offers superior image quality, the trade-off in computational complexity makes bilinear interpolation a more suitable choice for our specific research objectives.

3 Sentinel-1 Preprocessing

Preprocessing of Sentinel-1 SAR data is a vital initial step to enhance the data quality and prepare it for further analysis, including super resolution. This phase involves several essential procedures, namely Thermal/Border Noise Removal, Radiometric Calibration, and Speckle Filtering (Filipponi 2019). To perform these preprocessing tasks, we leverage the powerful applications QGIS³ and ESA SNAP⁴, which provide robust tools for efficiently handling SAR data.

Applying the orbit file is the initial step to ensure proper geolocation of the SAR data. Geolocation involves determining the precise position of the satellite and the corresponding Earth coordinates for each pixel in the image. Accurate geolocation is essential for aligning the SAR data with geographical coordinates and facilitating meaningful spatial analysis.

3.1 Thermal/Border Noise Removal

In SAR imagery, thermal and border noise can introduce unwanted variations and distortions, negatively impacting the quality of the images. Thermal noise arises from temperature fluctuations

³QGIS (Quantum Geographic Information System) is an open-source and freely available software designed for tasks such as creating, editing, visualizing, analyzing, and publishing geospatial information.

⁴SNAP (Sentinel Application Platform) toolbox is an accessible tool for Earth observation analysis, enabling exploration, analysis, and processing of remote-sensing data to support research, education, training, and operational applications.

in the sensor's electronics, while border noise results from differences in signal-to-noise ratios across the image. To tackle these issues, advanced filtering techniques are utilized, selectively reducing the influence of thermal and border noise. Removing such noise components significantly improves the overall image quality, ensuring more accurate subsequent analysis and super resolution.

3.2 Radiometric Calibration

Radiometric calibration is a crucial process in SAR preprocessing that transforms the raw digital numbers (DN) of SAR images into calibrated radiometric values (Moskolaï et al. 2022). This step involves correcting for sensor-specific characteristics and converting the DN values into meaningful backscatter intensity measurements expressed in decibels (dB). Calibrating the SAR data facilitates quantitative analysis, comparison with other SAR datasets, and consistency in subsequent processing steps, including super resolution.

3.3 Speckle Filtering

Speckle noise is a unique form of noise commonly observed in SAR images, caused by the coherent nature of radar waves (Singh and Shree 2016). This noise appears as a granular pattern, obscuring image details and hindering accurate interpretation. To address this issue, speckle filtering techniques are employed to reduce the noise while preserving essential structural information. Adaptive filters, such as Lee, Frost, or Gamma-MAP, are applied to smooth the image based on local statistics, effectively suppressing speckle noise without blurring important features.

Terrain Correction and Conversion to dB are also critical preprocessing steps in optimizing Sentinel-1 SAR data for analysis. Geometric distortions may occur due to variations in terrain elevation, affecting the accuracy of spatial representation (Small 2011). Terrain correction addresses these distortions by adjusting the image to compensate for topographical variations, ensuring precise alignment with geographical coordinates. Additionally, converting SAR data from the linear scale to a logarithmic scale, typically in decibels (dB), enhances the visibility of features with varying backscatter intensities, enabling easier analysis and interpretation of the SAR image.

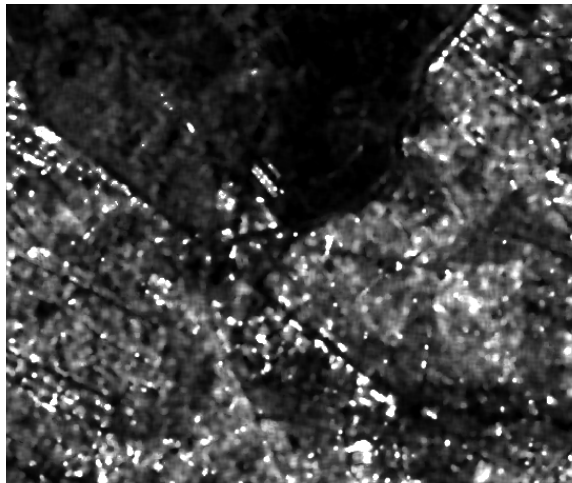


Figure 8: City Gaziantep: preprocessed Sentinel-1 SAR image

In conclusion, Sentinel-1 preprocessing, comprising mainly thermal/border noise removal, radiometric calibration, and speckle filtering, is crucial to optimize SAR image quality, eliminate unwanted artifacts, and prepare the data for successful super resolution. These preprocessing steps

ensure that the SAR data is suitably processed for further analysis and model training, thereby facilitating the investigation into the feasibility of generating high-resolution satellite images from lower-resolution inputs.

4 Approach 1: pairing Sentinel-1 data with Capella data

In this approach, we aim to leverage the complementary strengths of Sentinel-1 SAR data, offering extensive coverage but lower resolution, and Capella Space SAR data, providing higher resolution but limited scope. The objective is to create a unified dataset with consistent pixel size, enabling further analysis and exploration of machine learning techniques for super resolution in SAR imaging.

4.1 Image Resizing

In this step, we employ a dual-pronged approach to achieve pixel size uniformity. Firstly, we downscale the higher-resolution Capella SAR images to match the coarser resolution of Sentinel-1 images, resulting in a pixel size of 5 meters by 5 meters. Concurrently, we upscale the lower-resolution Sentinel-1 SAR images to adhere to the same 5 meters by 5 meters pixel size.

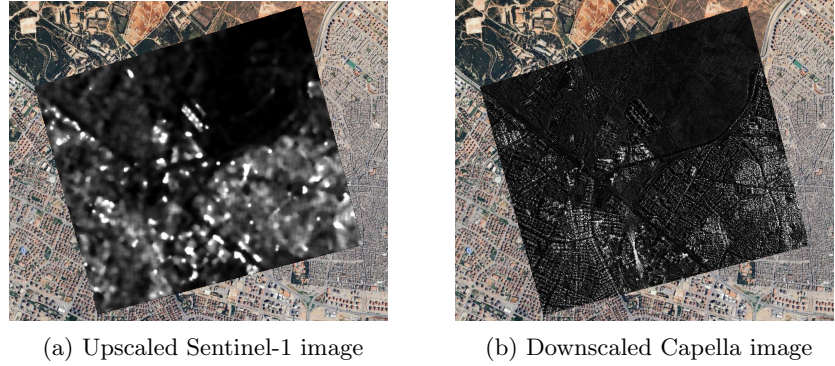
To achieve this, we perform a two-fold operation. Firstly, we downscale the higher-resolution Capella SAR images to match the pixel size of Sentinel-1 images, resulting in a consistent pixel size of 5 meters by 5 meters. This process entails the application of bilinear interpolation. Bilinear interpolation computes new pixel values by considering the weighted average of neighboring pixels. This method ensures a smooth transition while retaining relevant information, essential for preserving the integrity of the original Capella images.

Simultaneously, we upscale the lower-resolution Sentinel-1 SAR images to the same pixel size of 5 meters by 5 meters, using the same bilinear interpolation technique. This upscaling process ensures that the finer details present in Capella images can be accommodated in the resized Sentinel-1 images, enabling meaningful comparative analysis.

The uniform pixel size facilitates direct pixel-to-pixel comparison between the two datasets, essential for subsequent pixel alignment and coherent analysis. By harmonizing the pixel sizes, we establish a standardized platform for the exploration of machine learning techniques and super resolution strategies, enabling accurate evaluation and enhancement of SAR images from Sentinel-1 data.

4.2 Pixel Alignment

Pixel alignment is the subsequent step, where we focus on precisely aligning the resized Sentinel-1 images with the corresponding Capella images. As both datasets may have different spatial referencing and coordinate systems, it is essential to achieve accurate pixel-to-pixel alignment to facilitate meaningful analysis and feature extraction in later stages.



(a) Upscaled Sentinel-1 image

(b) Downscaled Capella image

Figure 10: The image pair generated by Approach 1

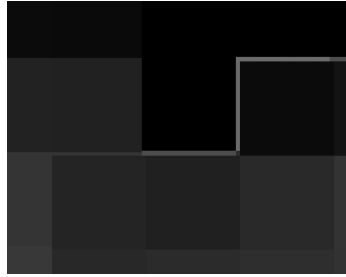


Figure 9: Image not aligned to pixels

To achieve pixel alignment, we employ georeferencing techniques and consider the spatial extent and coordinate reference systems (CRS) of both datasets. By performing geometric transformations on the Sentinel-1 images, we ensure that each pixel's location corresponds accurately to the corresponding pixel in the Capella images.

With this alignment in place, a pair of images emerges: the upscaled Sentinel-1 image and the downsampled Capella image. This image pair is central to our super resolution exploration. The upscaled Sentinel-1 image assumes the role of the feature input, possessing enhanced pixel resolution through the bilinear interpolation process. On the other hand, the downsampled Capella image serves as the label image, representing the high-resolution counterpart that we aim to approximate through our analysis.

This image pair encapsulates the essence of our approach. The synergy between the feature image and the label image forms the core framework for the application of machine learning models and advanced techniques. By utilizing the relationship between the two images, we embark on the journey to explore and develop strategies for super resolution in SAR imaging. The upscaled Sentinel-1 image encapsulates the potential for enhancing resolution, while the downsampled Capella image encapsulates the ground truth, offering the reference against which our super resolution models will be evaluated.

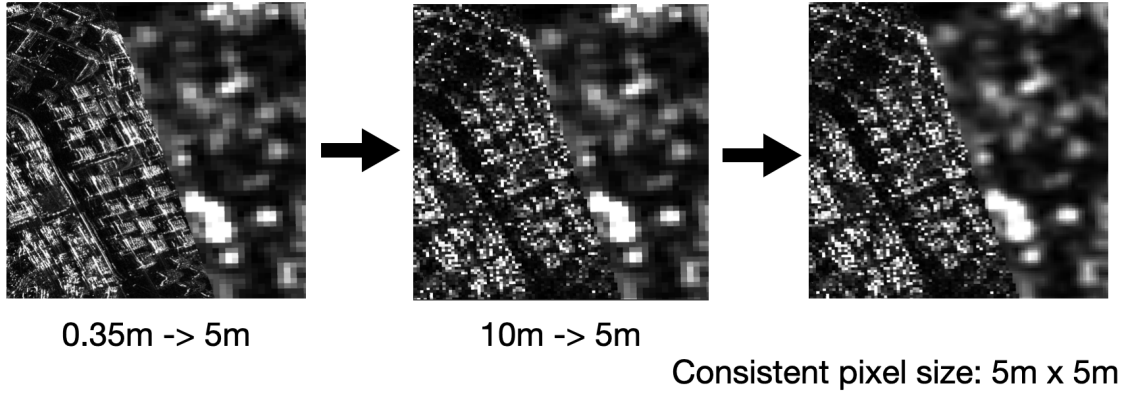


Figure 11: Approach 1 workflow

5 Approach 2: Simulate a Sentinel-1 Image Data

In this approach, we embark on a simulated journey to approximate Sentinel-1 SAR image data through a series of intricate transformations and enhancements. By harnessing the power of image processing techniques, we aim to construct a synthesized Sentinel-1 image that captures the essence of the real-world imagery provided by Capella Space.

5.1 Simulation Based on Capella Image

Our approach to simulating Sentinel-1 image data is marked by a series of intricate transformations designed to emulate the characteristics of real-world SAR imagery. To initiate this process, we address the challenge of balancing pixel size adjustments to capture the essence of Sentinel-1 data while maximizing efficiency and information retention.

Directly downscaling the original high-resolution Capella image to match the 10 meters by 10 meters pixel size of Sentinel-1 imagery presents certain limitations. While achieving consistency in pixel dimensions, this approach might result in the loss of finer details and intricacies inherent in the Capella image. Recognizing this trade-off, we adopt a more strategic method that balances both fidelity and efficiency.

In line with this strategic approach, we first downscale the Capella image to a pixel size of 5 meters by 5 meters. This decision, while deviating from the original Sentinel-1 pixel size, is a calculated choice. By halving the pixel size, we aim to retain a substantial portion of the Capella image's original detail while achieving compatibility with the Sentinel-1 image's dimensions.

Once we have downscaled the Capella image to the intermediary 5 meters by 5 meters pixel size, we embark on a subsequent upscale to an ultra-fine 1 meter by 1 meter pixel size, which represents the simulated sentinel-1 image. At the same time, we prepare a downscaled capella image with same 1 meter by 1 meter pixel size. In this way, the transformation aligns the simulated image's dimensions with those of our prepared Capella data, ensuring a seamless comparison and evaluation process. This resizing process not only simulate the finer details of Sentinel-1 imagery but also recognizes the inefficiency of direct downscaling, optimizing the trade-offs between pixel size and detail retention.

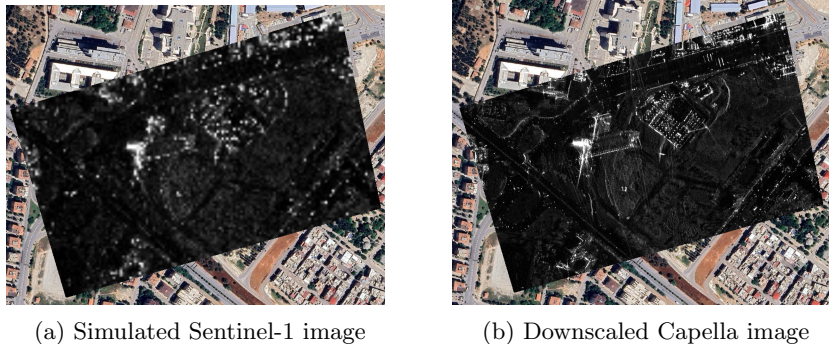


Figure 12: The image pair generated by Approach 2

5.2 Gaussian Blur and Image Entropy

In this critical stage of our approach, we delve into the intricate process of refining our simulated Sentinel-1 image to align with the characteristics of original Sentinel-1 image data. Our objective is to ensure that our simulated image not only possesses enhanced spatial resolution but also exhibits comparable textural properties and nuances to the authentic SAR imagery.

To achieve this, we initiate a meticulous comparison between the entropy of our simulated Sentinel-1 image and the entropy of the original Sentinel-1 image data. Image entropy serves as a valuable metric, quantifying the level of randomness or uncertainty within an image.

Mathematically, entropy is represented as:

$$\text{Entropy} = - \sum_{i=1}^N (p_i \cdot \log_2(p_i))$$

Here, p_i denotes the normalized histogram counts of the image, and N represents the total number of histogram bins. The calculation encapsulates the distribution of pixel values and their relative frequencies, allowing us to quantify the diversity and randomness present within the image.

By comparing the entropy values, we gain insight into the textural intricacies present in both images. Our aim is to ensure that our simulated image mirrors the textural patterns inherent in the original Sentinel-1 data.

To align the textural properties, we judiciously apply Gaussian blur to our simulated Sentinel-1 image. Gaussian blur is not only renowned for its ability to introduce a controlled degree of blurring but also for its capacity to preserve the overall structure of the image. Through iterative testing and adjustment, we fine-tune the parameters of the Gaussian blur to achieve an image entropy that closely matches that of the original Sentinel-1 image data.

With our refined and textured simulated image in hand, we proceed into the realm of machine learning armed with an asset that closely resembles authentic Sentinel-1 data. Through the subsequent stages, we unravel the potential of machine learning models to bring our simulated image closer to the desired super resolution objective.

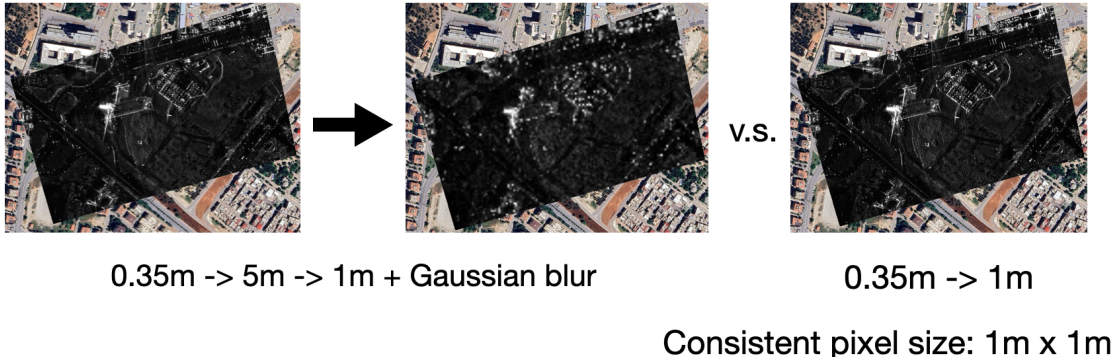


Figure 13: Approach 2 workflow

6 Machine Learning Models

In this section, we pivot our focus toward the application of machine learning models to tackle the super resolution challenge in SAR imaging. Recognizing the intrinsic complexity of this task, we harness the power of machine learning algorithms to bridge the resolution gap between our feature images and label images. Our selection encompasses the Random Forest, Gradient Boosting Random Forest, and Decision Tree models, each chosen for its distinct strengths and characteristics.

6.1 Model Selections

6.1.1 Random Forest

The Random Forest algorithm assembles an ensemble of decision trees to yield a potent predictive mechanism. Denote the set of decision trees as $\{\text{Tree}_1, \text{Tree}_2, \dots, \text{Tree}_T\}$, where T signifies the number of trees in the forest. Each decision tree Tree_t is constructed on a bootstrap sample of the training data and employs random feature selection (Hastie, Tibshirani, and Friedman 2004). The final prediction of the Random Forest is given by the ensemble average of individual tree predictions:

$$\text{RF Prediction} = \frac{1}{T} \sum_{t=1}^T \text{Tree}_t(\text{Sample})$$

Here, $\text{Tree}_t(\text{Sample})$ represents the prediction of the t -th decision tree on a specific sample. In the context of super resolution, the Random Forest model holds the potential to capture intricate relationships between the feature image and the label image. The model's ability to handle non-linear relationships and its resistance to overfitting align with the nuanced nature of SAR imagery.

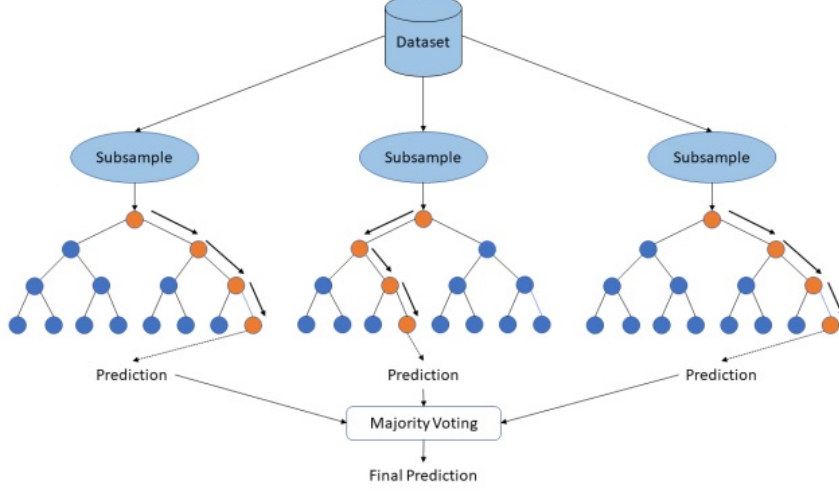


Figure 14: Random forest

6.1.2 Gradient Boosting Random Forest

Akin to an evolutionary leap from the conventional Random Forest, the Gradient Boosting Random Forest (GBRF) amalgamates the prowess of gradient boosting with the robust framework of a random forest. GBRF's essence lies in the sequential construction of decision trees, which enables the model to excel in addressing complex relationships within the data (Bonaccorso 2018). Represent the collection of GBRF trees as $\{\text{Tree}_1, \text{Tree}_2, \dots, \text{Tree}_T\}$. In this framework, each tree Tree_t aims to rectify the errors made by its predecessors. The final GBRF prediction is the summation of individual tree predictions:

$$\text{GBRF Prediction} = \sum_{t=1}^T \text{Tree}_t(\text{Sample})$$

Its adaptive learning mechanism positions it well to extract intricate features from our input image, striving for a comprehensive understanding of its alignment with the desired output image.

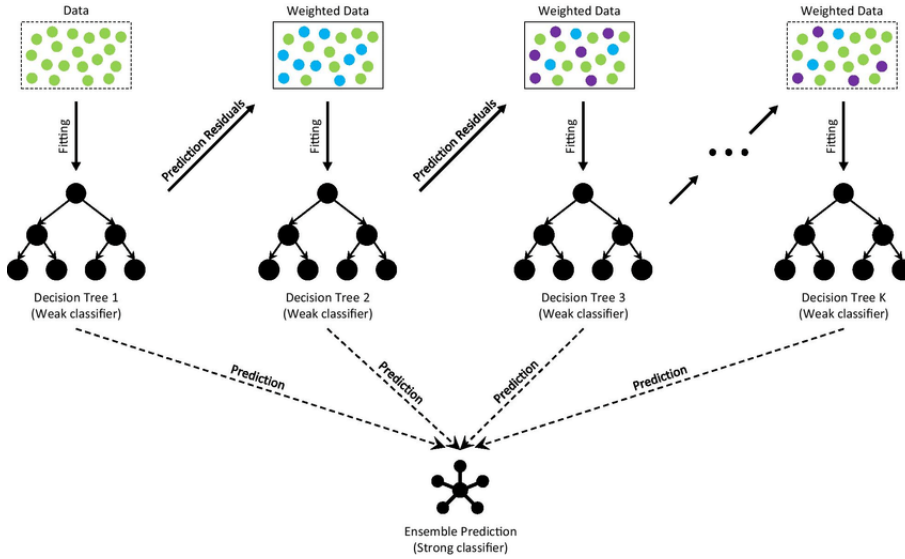


Figure 15: Gradient Boosting Random forest

6.1.3 Decision Tree

At the fundamental level, a Decision Tree forms the cornerstone of our ensemble models. Decision trees partition the data space through feature thresholds, delineating non-linear decision boundaries (Hastie, Tibshirani, and Friedman 2004). Consider a single decision tree DT. The prediction produced by traversing its paths and reaching a terminal node is given by:

$$\text{DT Prediction} = \text{Terminal Node Prediction}$$

Despite its simplicity, Decision Trees offer insights into the most significant attributes that influence the super resolution transformation. Its interpretability enables us to discern the critical variables that guide the enhancement process. By navigating the hierarchy of decisions, the Decision Tree model aims to uncover the pivotal factors contributing to successful super resolution, shedding light on the nuanced relationships within the data.

Each of these selected machine learning models possesses unique traits that synergize with the intricate nature of our super resolution challenge. In the subsequent sections, we delve into the preparation of feature vectors, the utilization of Principal Component Analysis, and the evaluation metrics that guide our assessment of these models' performance.

6.2 Feature Vectors Preparation

In the pursuit of super resolution through machine learning models, the crux lies in the preparation of feature vectors that encapsulate the essence of the input data. These vectors serve as the foundation upon which our models uncover the intricate relationships and patterns inherent within the images. Our approach to feature vector preparation involves a multi-dimensional integration of pertinent information.

6.2.1 Surrounding Pixel Values

First and foremost, we incorporate the neighboring pixel values surrounding each pixel in a 5x5 window. This holistic view captures the spatial context, allowing our models to comprehend the local relationships and nuances present within the images. By considering these surrounding pixel values, we empower our models to discern patterns that extend beyond individual pixels, thus enhancing the precision of our super resolution endeavor.

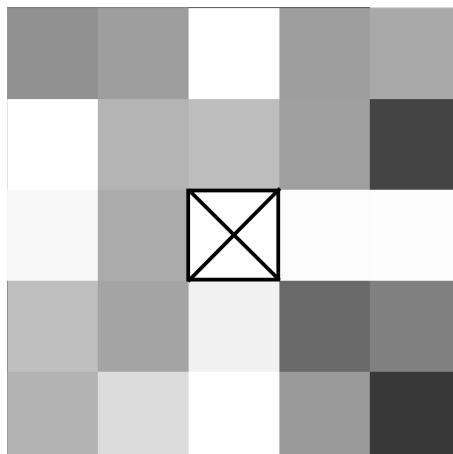


Figure 16: 5x5 window for a centre pixel

6.2.2 RGBI Band Pixel Values from Sentinel-2

In our quest to construct comprehensive feature vectors, we turn to the rich and varied spectral offerings of Sentinel-2 imagery. The Sentinel-2 satellite brings forth a tapestry of 13 spectral bands, each encapsulating unique insights into the Earth's surface (Drusch et al. 2012). Within this wealth of data, we hone in on four crucial bands—blue (B2), green (B3), red (B4), and near-infrared (B8)—each graced with a 10-meter pixel resolution. This addition provides a multispectral perspective, enriching the feature vectors with color and infrared information. The incorporation of these spectral bands offers a holistic representation of the scene's characteristics, augmenting the models' capacity to uncover intricate patterns and attributes.

Multiple band combinations from Sentinel-2 could be generated to highlight different features. One notable band combination is the natural color band combination, crafted from the red (B4), green (B3), and blue (B2) channels. This combination mirrors how the human eye perceives the world, presenting imagery in the familiar hues of reality. (See Figure 17)



Figure 17: City Gaziantep: the natural color band combination from Sentinel-2

6.2.3 Calculation of GNDVI, NDVI, and Building Index

Within our intricate feature vector preparation lies the calculation and exploration of essential vegetation and building indices. These indices distill vital environmental attributes, enriching our vectors with insights into vegetation health and the presence of built structures (Hill 2013).

One of these indices, the Green Normalized Difference Vegetation Index (GNDVI), encapsulates the vigor and health of vegetation. This index is computed as

$$\frac{NIR - Green}{NIR + Green},$$

where *NIR* stands for Near-Infrared reflectance and *Green* represents the green channel reflectance. GNDVI's value ranges between -1 and 1, with higher values indicating healthier and denser vegetation. This index serves as a valuable proxy for understanding vegetation distribution and health across the landscape.

Delving further into vegetation assessment, the Normalized Difference Vegetation Index (NDVI) offers insights into vegetation vigor and coverage. Calculated as

$$\frac{NIR - Red}{NIR + Red},$$

where *Red* symbolizes the red channel reflectance, NDVI's values span from -1 to 1. Elevated values signify robust vegetation presence, while lower values suggest sparse or stressed vegetation. NDVI acts as a versatile tool for monitoring vegetation dynamics, aiding our models in understanding the ecological makeup of the region.

Shifting our focus to built environments, the Building Index unveils the presence of constructed structures within the imagery. Computed as

$$\frac{Red - NIR}{Red + NIR},$$

where *Red* stands for the red channel reflectance and *NIR* denotes Near-Infrared reflectance, the Building Index yields values that illuminate urban landscapes and structures. Positive values signify building presence, while negative values denote non-built areas. This index offers a nuanced perspective on urbanization and human-made landscapes.

Through the computation of GNDVI, NDVI, and the Building Index, our feature vectors are infused with critical environmental insights. These indices, calculated from Sentinel-2's rich spectral offerings, broaden our understanding of vegetation health and built infrastructure. Armed with these indices, our machine learning models delve into uncovering intricate relationships and patterns, setting the stage for our subsequent model evaluations and analysis.

6.2.4 Integration of Building Layer from OpenStreetMap

Lastly, we integrate the building feature layer sourced from OpenStreetMap⁵, enriching the feature vectors with information about the built environment. This feature layer contributes spatial context, aiding our models in discerning the structural characteristics of the region (OpenStreetMap contributors 2017). By incorporating this data, we infuse the feature vectors with human-made landscape attributes, enhancing the depth and realism of our super resolution exploration.

The culmination of these multi-faceted elements forms our comprehensive feature vectors. By integrating surrounding pixel values, spectral information from Sentinel-2, vegetation indices, and building data, we construct a holistic representation that captures the intricate essence of the images. These feature vectors become the cornerstone upon which our machine learning models operate, endeavoring to extract underlying relationships and guide our super resolution mission toward success.

⁵OpenStreetMap employs an extensive tagging system to represent tangible elements like roads and buildings, associating descriptive attributes with fundamental data structures such as nodes, ways, and relations, wherein each tag signifies a relevant geographical attribute.

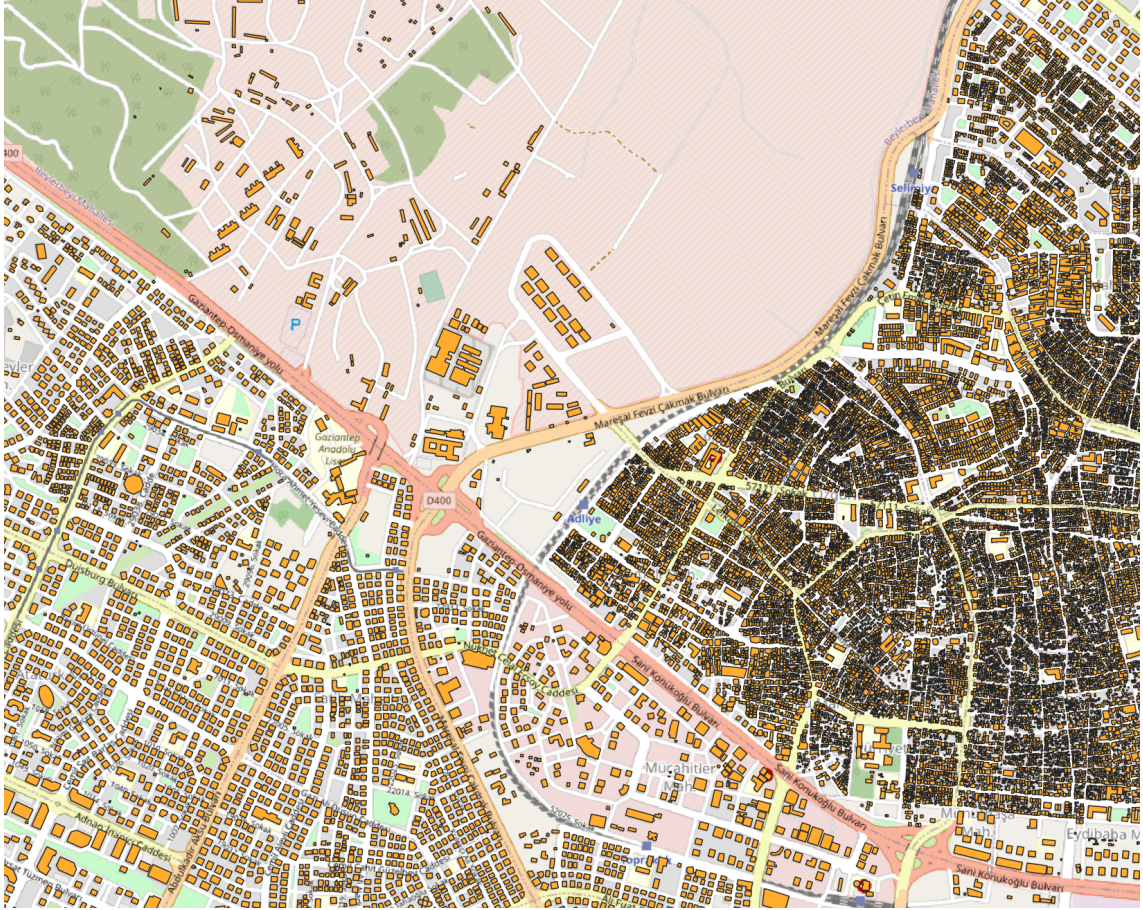


Figure 18: City Gaziantep: the building layer from Open Street Map.
Map data copyrighted OpenStreetMap contributors and
available from <https://www.openstreetmap.org>.

6.3 Principal Component Analysis

In the pursuit of unraveling the complex relationships embedded within our feature vectors, we turn to Principal Component Analysis (PCA) as a powerful technique for dimensionality reduction and pattern extraction (Jolliffe and Cadima 2016). The application of PCA is a pivotal step in our super resolution journey, as it transforms our multi-dimensional feature vectors into a reduced set of orthogonal components that capture the essence of the data.

PCA operates by projecting the original feature vectors onto a new orthogonal basis defined by the principal components. These components represent the directions of maximum variance within the data. By sorting these components based on their associated variances, we are able to capture the most significant patterns present in the feature vectors.

One of the key advantages of PCA lies in its ability to significantly reduce the dimensionality of our data. This reduction not only enhances computational efficiency but also aids in mitigating the "curse of dimensionality," a phenomenon that can lead to overfitting and diminished model performance when working with high-dimensional data (Hastie, Tibshirani, and Friedman 2004).

Furthermore, PCA serves to enhance the interpretability of our models by transforming the original features into a reduced set of principal components. These components represent combinations of

the original features, offering a more concise representation of the data while retaining its essential characteristics. The reduced dimensionality achieved through PCA allows our models to operate on a streamlined set of attributes, thereby promoting more robust and effective learning.

In our analysis, we introduce a novel approach by setting $n_components = 'mle'$, where ‘mle’ refers to the Maximum Likelihood Estimation, which automatically chooses the dimensionality for PCA. This technique, rooted in Bayesian model selection, facilitates the determination of the true dimensionality of the data (Minka 2000). By interpreting PCA as a density estimation task, this approach computationally infers the optimal number of principal components to retain.

In empirical assessments, this approach has demonstrated superior accuracy compared to conventional methods like cross-validation, while also exhibiting enhanced computational efficiency. Through the infusion of this advanced PCA strategy, our feature vectors achieve optimal dimensionality reduction, empowering our subsequent machine learning models to perform more effectively and efficiently.

Through the implementation of Principal Component Analysis, we aim to distill the intricate patterns and relationships embedded within our feature vectors. This reduction in dimensionality not only aids our models in achieving enhanced computational efficiency but also empowers them to focus on the most salient aspects of the data. In the subsequent sections, we delve into the evaluation metrics used to assess our model performance and present the results of our analysis, unveiling the potential of our machine learning-driven super resolution approach.

6.4 Evaluation Metrics for Model Performance

As we traverse the realm of machine learning-driven super resolution, a crucial aspect lies in the assessment of our model’s performance. In this pursuit, we employ well-established evaluation metrics that serve as yardsticks to gauge the effectiveness of our approach. One such metric that stands as a cornerstone in our analysis is the Mean Absolute Error (MAE).

MAE is a fundamental metric that quantifies the average absolute difference between the predicted values generated by our machine learning models and the corresponding ground truth values from our label images (Willmott and Matsuura 2005). This metric encapsulates the magnitude of the errors present within our super resolution predictions.

Mathematically, MAE is calculated as the average of the absolute differences between the predicted values \hat{y}_i and the actual values y_i :

$$MAE = \frac{1}{n} \sum_{i=1}^n |\hat{y}_i - y_i|$$

Here, n represents the total number of data points being evaluated. The lower the MAE, the closer the predictions align with the actual values, signifying higher accuracy and precision in our super resolution transformations.

By employing MAE as an evaluation metric, we gain a comprehensive understanding of how effectively our machine learning models bridge the resolution gap between the upscaled Sentinel-1 images and the true high-resolution Capella images. This metric allows us to quantitatively compare the performance of our models, shedding light on their ability to uncover intricate relationships

and patterns inherent within the SAR imagery. As we progress, armed with these evaluation insights, we unravel the success of our super resolution endeavor and delve into the results and analysis that mark the culmination of our exploration.

7 Results and Analysis

7.1 Approach 1: pairing Sentinel-1 data with Capella data

Figure 19 provides us with a visual glimpse of the outcome achieved through Bilinear Interpolation and our ensemble models.

Among the array of models employed, the Gradient Boosting Random Forest emerges as a standout performer, as evidenced by the lowest Mean Absolute Error (MAE). The minimized MAE underscores its adeptness in minimizing the disparities between the synthesized high-resolution images and the actual Capella images. Furthermore, the synthesized image produced by Gradient Boosting Random Forest exhibits a nuanced contrast, preserving crucial highlight points with subtle yet perceptible improvements.

In contrast, the image generated by the Random Forest model, while commendable, offers slightly lesser contrast when juxtaposed with Gradient Boosting Random Forest. This marginal distinction hints at the latter's capacity to encapsulate and amplify subtle details, fostering a more realistic visual rendition.

A discernable disparity is discerned when assessing the performance of the Decision Tree model. The synthesized image produced by this model exhibits a coarser texture, marked by less pronounced detail and a lack of well-defined pathways. Consequently, this model yields the highest MAE, denoting a comparative struggle in attaining congruence between the high-resolution synthetic image and the actual Capella image.

In summation, this initial approach underlines the pivotal role of ensemble models, especially the Gradient Boosting Random Forest, in effectively enhancing the resolution of the low-resolution Sentinel-1 images.

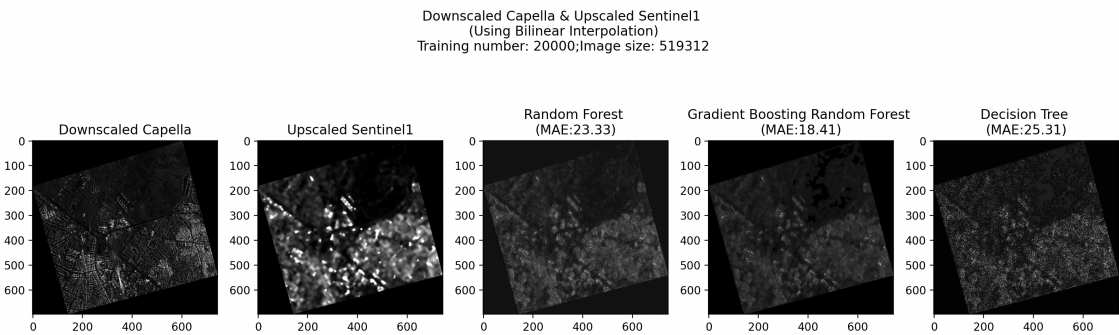


Figure 19: Predictions from different models (Bilinear interpolation).

7.1.1 Enhancing Super Resolution: EDSRx2 Upscaling

Continuing our quest for improved super resolution outcomes, we explore a fresh avenue by replacing the common Bilinear Interpolation method with the Enhanced Deep Residual Networks for Single Image Super-Resolution (EDSRx2) model during the upscaling process. This innovative

approach promises to bring about more intricate and refined high-resolution images, enhancing our pursuit of super resolution.

In the realm of deep learning, we turn our attention to the Enhanced Deep Residual Networks for Single Image Super-Resolution (EDSR) model, as outlined by (Lim et al. 2017). EDSR's capabilities are substantiated through its pre-training on the expansive DIV2K dataset, making it proficient in delivering high-quality super resolution results for various scaling factors. EDSR's primary objective revolves around enhancing high-resolution (HR) images using individual low-resolution (LR) counterparts. This feat is accomplished by harnessing the potential of deep residual networks, renowned for their adeptness in comprehending intricate patterns and capturing subtle nuances.

This strategic adaptation aimed to harness the enhanced capabilities of EDSRx2 in the pursuit of superior results. The consequential impact of this transition is vividly illustrated in Figure 20.

A perceptible evolution is palpable across all models, reaffirming the efficacy of our strategic alteration. The transformation is most apparent in the upper-right quadrant of the images, where a previously latent pathway now emerges distinctly. Roads and blocks are meticulously outlined, forming coherent patterns that were previously elusive. The visual landscape attains a newfound smoothness, enhancing the seamless alignment of the highlight segments with the corresponding segments in the Capella images.

This transformative augmentation reverberates across the entire visual expanse, generating outcomes that are both visually refined and perceptually enriched. The synthesis of a tangible path, the precision of road and block delineation, the emergence of intricate patterns, and the seamless amalgamation of highlight segments collectively substantiate the qualitative advancements brought forth by the adoption of EDSRx2.

This transformation underscores the malleability and adaptability of our super resolution approach, wherein the meticulous choice of techniques and methodologies plays a pivotal role in sculpting the resultant images.

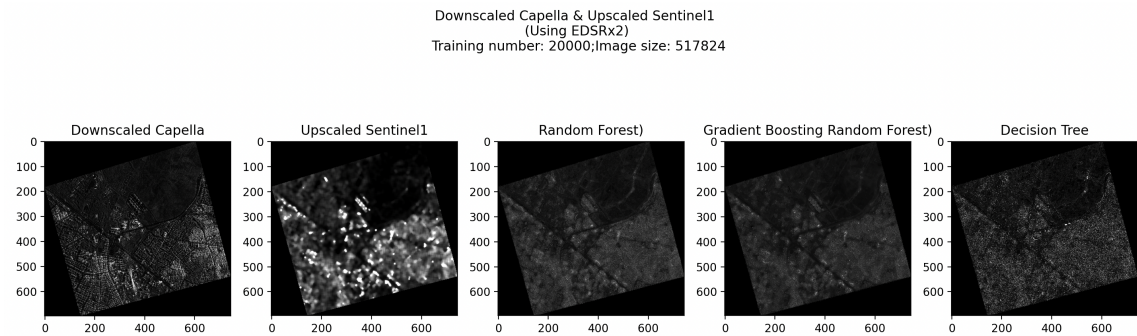


Figure 20: Predictions from different models (EDSRx2).

7.2 Approach 2: Simulate a Sentinel-1 Image Data

Moving forward, we delve into Approach 2, a method that necessitates a more focused strategy due to its unique requirements. In this scenario, obtaining high-resolution images raises efficiency concerns, leading us to adopt a practical approach of cropping and zooming into specific areas with notable features like paths and buildings.

Figure 21 visually represents the outcomes of our approach. A careful examination of the images reveals that there is no significant improvement across the models we employed. Instead, each model seems to dim highlights and display a coarser appearance. This might seem unexpected, but it opens the door for deeper exploration.

We believe that this modest outcome could be due to the limited set of factors we considered and the specific area we focused on. This prompts us to explore further possibilities. By including more factors, trying different methods, or a combination thereof, we might achieve better results.

It's important to note that while the current results suggest room for improvement, Approach 2 still holds promise. It's an area ripe for further investigation. The idea of expanding our training dataset is particularly intriguing. This means we can harness the potential of more advanced computational resources to enhance our research.

In essence, Approach 2 presents both challenges and opportunities. While the current outcomes point to areas where we can refine our methods, the potential of this approach remains strong. This paves the way for future exploration and improvement, as we consider a range of technical, methodological, and computational enhancements in our ongoing pursuit of super resolution excellence.

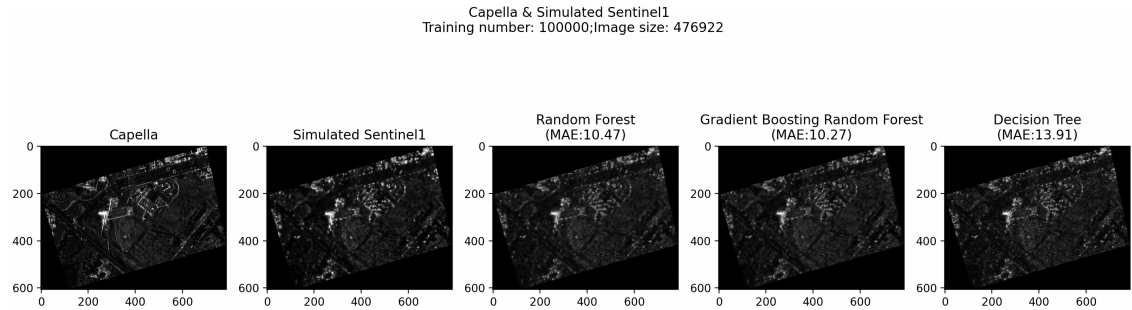


Figure 21: Approach 2: Predictions from different models.

8 Conclusion

As we reach the conclusion of our investigation, we come across constraints that demand careful contemplation. Notably, the scarcity of high-resolution Synthetic Aperture Radar (SAR) images akin to Capella's poses a constraint. Consequently, we rely on super resolution methods to upscale low-resolution images, effectively simulating the presence of high-resolution images within our feature vectors. The outcome of this process is contingent on the effectiveness of these methods.

Our outcomes could be further enhanced with access to a more expansive repository of high-resolution SAR images for specific regions. The presence of high-resolution images for a singular area or the availability of high-resolution and low-resolution image pairs for multiple locations could yield improved results. This underscores the potential of augmenting our dataset to facilitate more accurate super resolution.

Comparing our two approaches, Approach 1 exhibits promise that warrants deeper exploration. Given its inherent efficiency and the promising outcomes it has already produced, a more comprehensive study in this direction seems prudent. The integration of feature layers, tailored to the characteristics of each area, emerges as a potent tool for bolstering model training. For instance,

in the case of the focus area Gaziantep, a building layer could significantly enhance model performance. In parallel, similar considerations for other locations, such as incorporating highway or waterway layers, stand to benefit respective training processes.

The results derived from Approach 1, achieved through training on a single image, are inherently encouraging. This provides a robust foundation for further forays into the realm of super resolution. As our exploration unravels, the potential to substantially enhance the resolution of SAR images emerges as a captivating trajectory, warranting sustained attention and continued research efforts.

References

- Ager, Thomas (June 2013). “An Introduction to Synthetic Aperture Radar Imaging”. In: *Oceanography* 26.2. DOI: <https://doi.org/10.5670/oceanog.2013.28>.
- Amara, M, R Bandara, and Thushari Silva (2018). *SLIC Based Digital Image Enlargement*. URL: <https://arxiv.org/pdf/1810.02643.pdf>.
- Berens, Patrick (2006). *Introduction to Synthetic Aperture Radar (SAR)*, pp. 3–4. URL: <https://www.sto.nato.int/publications/STO%20Educational%20Notes/RTO-EN-SET-086/EN-SET-086-03.pdf>.
- Bing, Lei et al. (Sept. 2019). “Spatial Distribution Characteristics of Oil Spills in the Bohai Sea Based on Satellite Remote Sensing and GIS”. In: *Journal of Coastal Research* 90.sp1, p. 164. DOI: <https://doi.org/10.2112/si90-020.1>.
- Bonaccorso, Giuseppe (2018). *Machine learning algorithms : popular algorithms for data science and machine learning*. Birmingham, U.K.: Packt Publishing Ltd. ISBN: 9781789347999.
- Capella (June 2023). *What SAR imagery products are available with Capella?* URL: <https://support.capellaspace.com/hc/en-us/articles/360059224291-What-SAR-imagery-products-are-available-with-Capella->.
- Drusch, M. et al. (May 2012). “Sentinel-2: ESA’s Optical High-Resolution Mission for GMES Operational Services”. In: *Remote Sensing of Environment* 120, pp. 25–36. DOI: <https://doi.org/10.1016/j.rse.2011.11.026>. URL: <https://www.sciencedirect.com/science/article/pii/S0034425712000636>.
- ESA (n.d.). *User Guides - Sentinel-1 SAR - Product Types and Processing Levels - Sentinel Online*. URL: <https://sentinels.copernicus.eu/web/sentinel/user-guides/sentinel-1-sar/product-types-processing-levels>.
- Filipponi, Federico (June 2019). “Sentinel-1 GRD Preprocessing Workflow”. In: *Proceedings* 18.1, p. 11. DOI: <https://doi.org/10.3390/ecrs-3-06201>.
- Freeman, Diana, David Green, and David Hassell (1994). “A guide to Geographic Information Systems (GIS)”. In: *Teaching Geography* 19.1, pp. 36–37. URL: https://www.jstor.org/stable/23754584?searchText=raster+image&searchUri=%2Faction%2FdoBasicSearch%3FQuery%3Draster%2Bimage&ab_segments=0%2Fbasic_search_gsv%2Fcontrol&refreqid=fastly-default%3Aed7763bf975c4727eef8cb9ce5c71e34.
- Hastie, Trevor, Robert Tibshirani, and J H Friedman (2004). *The elements of statistical learning : data mining, inference, and prediction : with 200 full-color illustrations*. New York: Springer. ISBN: 9780387952840.
- Hill, Michael D (Oct. 2013). “Vegetation index suites as indicators of vegetation state in grassland and savanna: An analysis with simulated SENTINEL 2 data for a North American transect”. In: *Remote Sensing of Environment* 137, pp. 94–111. DOI: <https://doi.org/10.1016/j.rse.2013.06.004>.
- Jolliffe, Ian T. and Jorge Cadima (2016). “Principal component analysis: a review and recent developments”. In: *Philosophical Transactions: Mathematical, Physical and Engineering Sciences* 374.2065, pp. 1–16. URL: https://www.jstor.org/stable/24760364?searchText=pca&searchUri=%2Faction%2FdoBasicSearch%3FQuery%3Dpca&ab_segments=0%2Fbasic_search_gsv%2Fcontrol&refreqid=fastly-default%3Ab5e1727f91cf4b034b0aaf9827

- Kuchkorov, Temurbek et al. (Nov. 2020). “Satellite image formation and preprocessing methods”. In: *2020 International Conference on Information Science and Communications Technologies (ICISCT)*. DOI: <https://doi.org/10.1109/icisct50599.2020.9351456>.
- Li, Yanshan et al. (Oct. 2021). “OGSRN: Optical-guided super-resolution network for SAR image”. In: *Chinese Journal of Aeronautics*. DOI: <https://doi.org/10.1016/j.cja.2021.08.036>.
- Lim, Bee et al. (July 2017). “Enhanced Deep Residual Networks for Single Image Super-Resolution”. In: *arXiv:1707.02921 [cs]*. URL: <https://arxiv.org/abs/1707.02921>.
- Menezes, Elizabeth Ashley and Magali Barba-Sevilla (Jan. 2023). *GUIDE: FUNDAMENTALS OF SYNTHETIC APERTURE RADAR (SAR)*. URL: <https://storymaps.arcgis.com/stories/20d8cd2ce11a4d5d81a8a65711d5ec29>.
- Minka, Thomas.P (Dec. 2000). “Automatic choice of dimensionality for PCA”. In: pp. 598–604. URL: <https://tminka.github.io/papers/pca/minka-pca.pdf>.
- Moskolaï, Waytehad et al. (Oct. 2022). “A Workflow for Collecting and Preprocessing Sentinel-1 Images for Time Series Prediction Suitable for Deep Learning Algorithms”. In: *Geomatics* 2.4, pp. 435–456. DOI: <https://doi.org/10.3390/geomatics2040024>.
- Müller, M. U. et al. (Aug. 2020). “SUPER-RESOLUTION OF MULTISPECTRAL SATELLITE IMAGES USING CONVOLUTIONAL NEURAL NETWORKS”. In: *ISPRS Annals of the Photogrammetry, Remote Sensing and Spatial Information Sciences* V-1-2020, pp. 33–40. DOI: <https://doi.org/10.5194/isprs-annals-v-1-2020-33-2020>.
- NASA (2019). *SAR Handbook: Comprehensive Methodologies for Forest Monitoring and Biomass Estimation*. URL: <https://www.servirglobal.net/Global/Articles/Article/2674/sar-handbook-comprehensive-methodologies-for-forest-monitoring-and-biomass-estimation>.
- (n.d.). *What is Synthetic Aperture Radar?* URL: <https://www.earthdata.nasa.gov/learn/backgrounder/what-is-sar>.
- OpenStreetMap contributors (2017). *Planet dump retrieved from https://planet.osm.org*. URL: <https://www.openstreetmap.org>.
- özdemir, Caner (2012). *Inverse synthetic aperture radar imaging with MATLAB*. Hoboken, NJ: Wiley. ISBN: 9780470284841.
- Sanderson, Peta G. (Feb. 2001). “The Application of Satellite Remote Sensing to Coastal Management in Singapore”. In: *AMBIO: A Journal of the Human Environment* 30.1, pp. 43–48. DOI: <https://doi.org/10.1579/0044-7447-30.1.43>.
- Sekar, K R, V Duraisamy, and A M Remimol (Mar. 2014). “An approach of image scaling using DWT and bicubic interpolation”. In: *2014 International Conference on Green Computing Communication and Electrical Engineering (ICGCCEE)*. DOI: <https://doi.org/10.1109/icgccee.2014.6922406>.
- Singh, Prabhishiek and Raj Shree (Sept. 2016). “Analysis and effects of speckle noise in SAR images”. In: *2016 2nd International Conference on Advances in Computing, Communication, Automation (ICACCA) (Fall)*. DOI: <https://doi.org/10.1109/icaccaf.2016.7748978>.
- Singh, Prabhishiek and Raj Shree (Aug. 2018). “A new SAR image despeckling using directional smoothing filter and method noise thresholding”. In: *Engineering Science*

- and Technology, an International Journal* 21.4, pp. 589–610. DOI: <https://doi.org/10.1016/j.jestch.2018.05.009>.
- Small, David (Aug. 2011). “Flattening Gamma: Radiometric Terrain Correction for SAR Imagery”. In: *IEEE Transactions on Geoscience and Remote Sensing* 49.8, pp. 3081–3093. DOI: <https://doi.org/10.1109/tgrs.2011.2120616>.
- Smith, Laurence C. (Sept. 2002). “Emerging Applications of Interferometric Synthetic Aperture Radar (InSAR) in Geomorphology and Hydrology”. In: *Annals of the Association of American Geographers* 92.3, pp. 385–398. DOI: <https://doi.org/10.1111/1467-8306.00295>.
- Szeliski, Richard (2011). *Computer vision : algorithms and applications*. London: Springer. ISBN: 9781848829343.
- Weiser, Alan and Sergio E. Zarantonello (1988). “A Note on Piecewise Linear and Multilinear Table Interpolation in Many Dimensions”. In: *Mathematics of Computation* 50.181, pp. 189–196. DOI: <https://doi.org/10.2307/2007922>. URL: https://www.jstor.org/stable/2007922?searchText=bilinear+interpolation&searchUri=%2Faction%2FdoBasicSearch%3FQuery%3Dbilinear%2Binterpolation&ab_segments=0%2Fbasic-search_gsv2%2Fcontrol&refreqid=fastly-default%3A9b57412472babbbab9da21bd20add502.
- Willmott, CJ and K Matsuura (2005). “Advantages of the mean absolute error (MAE) over the root mean square error (RMSE) in assessing average model performance”. In: *Climate Research* 30.1, pp. 79–82. DOI: <https://doi.org/10.3354/cr030079>. URL: <https://www.int-res.com/articles/cr2005/30/c030p079.pdf>.
- Zhang, Chongqi et al. (Jan. 2023). “Blind Super-Resolution for SAR Images with Speckle Noise Based on Deep Learning Probabilistic Degradation Model and SAR Priors”. In: *Remote Sensing* 15.2, p. 330. DOI: <https://doi.org/10.3390/rs15020330>.
- Zhang, Lixian et al. (July 2021). “Making Low-Resolution Satellite Images Reborn: A Deep Learning Approach for Super-Resolution Building Extraction”. In: *Remote Sensing* 13.15, p. 2872. DOI: <https://doi.org/10.3390/rs13152872>.
- Zhang, Yongbing et al. (Nov. 2011). “Interpolation-Dependent Image Downsampling”. In: *IEEE Transactions on Image Processing* 20.11, pp. 3291–3296. DOI: <https://doi.org/10.1109/tip.2011.2158226>.